Molecular Beam Studies of Weak Interactions for Open Shell Systems: Spin–Orbit Dependence of the Potential Energy Surface for $O(^3P)$ with H_2 and CH_4

Vincenzo Aquilanti,* Roberto Candori, Leonardo Mariani, Fernando Pirani,

Dipartimento di Chimica dell'Università, 06100 Perugia, Italy

and Giorgio Liuti

Dipartimento di Chimica dell'Università, 53100 Siena, Italy *(Received: April 6, 1988)*

Molecular beam scattering studies of open shell atoms with analysis of magnetic sublevels provide information on the dependence from spin–orbit interaction of the long-range part of potential energy surfaces. From integral cross sections at thermal energies, quantitative information is derived both on the adiabatic surfaces and on the nonadiabatic coupling terms for the interactions of oxygen atoms in their ground state with molecular hydrogen and methane. Scattering data are also reported, and information relating to the van der Waals interaction is derived for the molecular hydrogen–molecular oxygen system.

I. Introduction

The extension of molecular beam scattering measurements beyond the closed shell atom–atom systems is an important step forward in obtaining intermolecular potentials for more complicated interactions, such as the chemically interesting ones of open shell atoms with diatomic and polyatomic molecules.[1-5]

The considerable experimental and theoretical difficulties encountered in obtaining meaningful data and reliable information on these systems have not hindered the efforts devoted to improving our knowledge of these van der Waals forces, which are relevant for the understanding of several microscopic and macroscopic phenomena.

Specifically, for studies involving open shell atoms, the useful theoretical framework recently proposed,[6-8] together with the experimental data obtained from scattering experiments where the open shell atom is in well-defined states, allows an accurate characterization of the weak interactions involved.[3-5,9,10]

Among the chemically interesting cases, where the determination of the potential energy surface is important also at the van der Waals asymptotic regions, the systems O–H_2 and O–CH_4 have a particular relevance. These surfaces can be profitably used in dealing with important processes such as combustion, flames, lasers, and atmospheric chemistry. A further motivation for such investigation is that a deeper knowledge of interactions involving open shell species allows a better assessment of orientation and alignment effects in reactive collisions when dominated by anisotropy at long range.

The reactive collisions of CH_4 and H_2 with the electronically metastable $O(^1D)$ have been studied extensively, in particular by Lee and co-workers[11] in a crossed molecular beam apparatus. From these studies interesting information on the dynamics and the initial mechanism of the reactions has been obtained. However, no scattering data have been reported for the $O(^3P)$–H_2 system, while for the $O(^3P)$–CH_4 system integral cross sections, in the thermal energy range, have been recently measured in this laboratory[12] and preliminary analyzed in terms of a single effective potential.

In this work we report the results obtained by measuring the absolute integral cross sections for the collisions of $O(^3P_j)$ with D_2 using a molecular beam apparatus. In the case of $O(^3P_j)$ atoms, a characterization of magnetic sublevels can be achieved by means of inhomogeneous magnetic fields. These data are analyzed together with those recently reported for O–CH_4,[12] in terms of an adiabatic analysis, which uses six effective potential energy curves correlating with the different atomic sublevels of the ground-state oxygen atom.

In the present experiment, D_2 has been chosen instead of H_2 as the target gas, because it allows a better experimental resolution for energy; also, as will be shown later, the adiabatic analysis is simplified.

These scattering studies, at the thermal energies used, give information on the potentials in the region of van der Waals wells. Therefore it is meaningful to study these weak long-range interactions by this technique, since energy barriers for possible chemical processes are sufficiently high (of the order of ten kcal/mol)[11,13,14] to forbid the occurrence of reactive collisions.

On the other hand, the integral cross section data for $O(^3P)$–D_2 and $O(^3P)$–CH_4 systems are amenable to practicable calculation procedures mostly because, under the experimental conditions of this work, the anisotropy of the D_2 and CH_4 molecules plays only a minor role.[12,15,16] Hence any anisotropy effect possibly observed can be attributed to the behavior of the oxygen atom.

The paper proceeds as follows: section II outlines the experimental apparatus and conditions, the theoretical framework for the analysis of results is presented in section III, and section IV reports the results and their analysis. A discussion of the features of the interactions obtained in this work, including a comparison with related work on O–rare gas systems,[9] is presented in section V. In the Appendix, the scattering data of the D_2–O_2 system, which have been measured for calibration of the absolute value of the cross sections involving D_2, will also be reported, and information will be provided on the spherical potential for the interaction between hydrogen and oxygen molecules.

(1) (a) Maitland, G. C.; Rigby, M.; Smith, E. B.; Wakeham, W. A. *Intermolecular Forces*; Oxford University Press, Oxford, U.K., 1981. (b) Scoles, G. *Ann. Rev. Phys. Chem.* **1980**, *31*, 81.
(2) Casavecchia, P.; He, G.; Sparks, R. K.; Lee, Y. T. *J. Chem. Phys.* **1982**, *77*, 1878 and references therein.
(3) Aquilanti, V.; Grossi, G.; Pirani, F. *Electronic and Atomic Collisions*; Invited Papers XIII ICPEAC; Eichler, J., Hertel, I. V., Stolterfoht, N., Eds.; Berlin, 1983; p 441.
(4) Vecchiocattivi, F. *Comments At. Mol. Phys.* **1986**, *17*, 163.
(5) Aquilanti, V.; Pirani, F.; Vecchiocattivi, F. *Structure and Dynamics of Weakly Bound Molecular Complexes*; Weber, A., Ed.; Plenum: New York, 1987; p 423.
(6) Aquilanti, V.; Grossi, G. *J. Chem. Phys.* **1980**, *73*, 1165.
(7) Aquilanti, V.; Casavecchia, P.; Grossi, G.; Laganà, A. *J. Chem. Phys.* **1980**, *73*, 1173.
(8) Aquilanti, V.; Grossi, G. Laganà, A. *Nuovo Cimento Soc. Ital. Fis., B* **1981**, *63B*, 7.
(9) Aquilanti, V.; Candori, R.; Pirani, F. *J. Chem. Phys.*, in press.
(10) Aquilanti, V.; Luzzatti, E.; Pirani, F.; Volpi, G. G. *Chem. Phys. Lett.* **1982**, *90*, 382; *J. Chem. Phys.*, in press.
(11) (a) Casavecchia, P.; Buss, R. J.; Sibener, S. J.; Lee, Y. T. *J. Chem. Phys.* **1980**, *73*, 6531. (b) Buss, R. J.; Casavecchia, P.; Hirooka, T.; Sibener, S. J.; Lee, Y. T. *Chem. Phys. Lett.* **1981**, *82*, 386.
(12) Liuti, G.; Pirani, F. *J. Chem. Phys.* **1987**, *87*, 5266.
(13) Wagner, A. F.; Bowman, J. M. *J. Chem. Phys.* **1987**, *86*, 1976.
(14) (a) Andresen, P.; Luntz, A. C.; *J. Chem. Phys.* **1980**, *72*, 5842. Luntz, A. C.; Andresen, P.; *J. Chem. Phys.* **1980**, *72*, 5851. Tsang, W.; Hampson, R. F. *J. Phys. Chem. Ref. Data* **1986**, *15*, 1087 and references therein.
(15) Liuti, G.; Luzzatti, E.; Pirani, F.; Volpi, G. G. *Chem. Phys. Lett.* **1987**, *135*, 387.
(16) For the behavior of D_2 see the Appendix of this work.

0022-3654/89/2093-0130$01.50/0

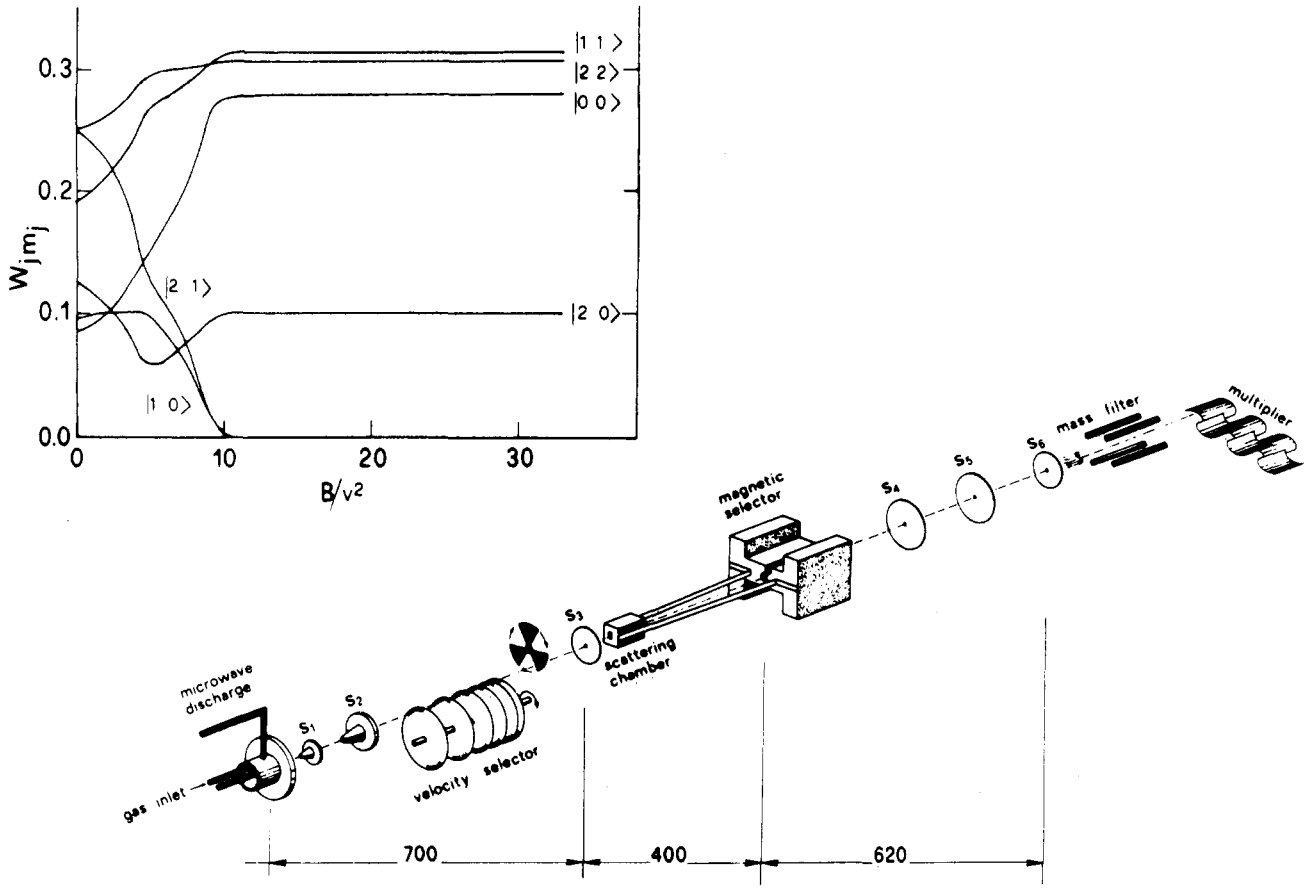

Figure 1. Schematic view of the apparatus for integral cross section measurements (all dimensions are in millimeters). The diameter of the collimating slits, which separate differentially pumped chambers, are 1.5 mm for S_1, S_2, S_5, and S_6, 0.7 mm for S_3, and 1.0 mm for S_4. The relative weights W_{jm_j} of the $|jm_j\rangle$ states of O atoms (see text and also Table I) as a function of magnetic induction B and velocity v are also shown. The values of the reduced parameter B/v^2 are in 10^2 G km^{-2} s^2.

II. Experimental Section

Measurements of absolute integral cross sections for atomic collisions in the thermal energy range have been carried out in this laboratory with the experimental arrangement schematized in Figure 1. This apparatus is basically the same as used in previous experiments.[3,9,10,12,17] The general conditions used in the O–D_2 experiment are the same as in the O–CH_4 case, and they are described in ref 12. The absolute values of the cross sections have been obtained with the same method previously described.[12] They involve a measurement of D_2–O_2 cross sections under the same experimental conditions: these measurements are reported in the Appendix, where it is also shown that they contain information on van der Waals forces. It has to be noted that these experiments using H_2 would have involved a large background noise in the mass spectrometric detector.

A Stern–Gerlach magnet (Rabi configuration, see ref 18a) allows the state analysis of the oxygen atom beam, which gives information on the atomic levels involved and allows a characterization of the polarization states;[18] this technique has been used in experiments involving nitrogen,[19] oxygen,[3,9,17b] and fluorine[3,5,10] atoms. For oxygen atoms, the magnetic analysis shows that a pure beam of ground-state ^3P_j atoms can be obtained by microwave discharge on O_2: the atom beam is essentially free of the possible metastable O($^1D_2$).[9] Figure 1 also shows that by varying the magnetic field strength at fixed velocity, it is possible to vary the composition of $|j\ m_j\rangle$ states which are transmitted by the magnetic analyzer. For this analysis, it is taken into account that j ($\mathbf{j} = \mathbf{L} + \mathbf{S}$) is a good quantum number for oxygen atoms in this range of magnetic fields, and m_j is its projection along the beam direction.[20] Specifically, for O(^3P_j), the electronic angular momentum $L = 1$ and the electronic spin $S = 1$ add to $j = 0,1,2$. Therefore, the use of magnetic selection allows one to perform cross section measurements with different sublevel populations.[21]

III. Theoretical Framework

The theory needed to interpret the experimental results and to obtain information on the interactions has been given and reviewed elsewhere.[3,5-8] Basically, the interaction, at a given total angular momentum J, is the sum of the following three contributions depending on the intermolecular distance R:

$$U^J(R) = V_{so}(R) + V_{el}(R) + V_{rot}(R)$$

For these low-energy processes, the dimension of the basis is conveniently restricted to the fine structure components, which are split asymptotically by the spin–orbit interaction of the open shell atom, V_{so}; the collision effects are described by the electrostatic interaction between the particles, V_{el}, which is relatively

(17) (a) Aquilanti, V.; Liuti, G.; Pirani, F.; Vecchiocattivi, F.; Volpi, G. G. *J. Chem. Phys.* **1976**, *65*, 4751. (b) Aquilanti, V.; Luzzatti, E.; Pirani, F.; Volpi, G. G. *J. Chem. Phys.* **1980**, *73*, 1181. (c) Brunetti, B.; Liuti, G.; Luzzatti, E.; Pirani, F.; Vecchiocattivi, F. *J. Chem. Phys.* **1981**, *74*, 6734. (d) Aquilanti, V.; Candori, R.; Luzzatti, E.; Pirani, F.; Volpi, G. G. *J. Chem. Phys.* **1986**, *85*, 5377.

(18) (a) Ramsey, N. F. *Molecular Beams*; Clarendon: Oxford, U.K., 1956. (b) Berkling, K.; Schlier, Ch.; Toshek, P. *Z. Phys.* **1962**, *168*, 81. (c) Fluendy, M. A. D.; Lawley, K. P. *Chemical Applications of Molecular Beam Scattering*; Chapman and Hall: London, 1973. (d) Aquilanti, V.; Pirani, F.; Luzzatti, E.; Volpi, G. G. *Gazz. Chim. Ital.* **1980**, *110*, 57. (e) Hishinuma, H.; Sueoka, O. *Chem. Phys. Lett.* **1983**, *98*, 414; **1985**, *121*, 293. (f) Reuss, G. *Atomic and Molecular Beams Method*; Scoles, G., Ed.; Oxford: New York, 1988.

(19) Brunetti, B.; Liuti, G.; Pirani, F.; Luzzatti, E. *Chem. Phys. Lett.* **1981**, *84*, 201.

(20) The beam direction is the natural collision quantization axis for the present experiments (see section III). Therefore, states defined in the laboratory system with the quantization axis along the magnetic field direction are related to states in the collision frame with the quantization axis along the beam direction by a suitable transformation matrix. It can be seen that, in this case, a rotation of the reference axis $\pi/2$ is necessary (see also ref 9, 10, and 17b).

(21) For more details on the magnetic analysis, see ref 9, 10, and 17b.

short-ranged, and by the centrifugal term $\mathbf{V}_{rot}$. These terms have a markedly different dependence on R: $\mathbf{V}_{so}$ slowly varies at the long range sampled by our experiments, $\mathbf{V}_{el}$ dies out exponentially, and $\mathbf{V}_{rot}$ decays as R^{-2}. According to the relative importance of these three terms, five alternative representations are possible, corresponding to different coupling schemes for the angular momenta involved (Hund's cases).

The choice of representations and recipes for simplifications based on decoupling schemes has been given elsewhere.[3,6,7] The simplification considered in the following is justified by the large spin–orbit splitting of the ground-state oxygen atom with respect to centrifugal effects. At the relatively small impact parameters relevant for glory scattering, this allows us to restrict our attention to only two cases: the molecular case (a) and the diatomic case (c), valid at short and long range, respectively, when the electrostatic interaction is stronger or respectively weaker than spin–orbit splitting. A proper label for scattering states is then $|j\ \Omega\rangle$ where j is the atomic angular momentum and Ω is the absolute value of its projection along the R axis. In this centrifugal sudden or coupled states (CS) decoupling scheme, the Ω quantum numbers are conserved[22] and the scattering at the energy E, considered as involving adiabatic effective potential curves, is described in the adiabatic representation by radial coupled Schrödinger equations:

$$\left[-\frac{\hbar^2}{2\mu}\left(\mathbf{I}\frac{\mathrm{d}}{\mathrm{d}R} + \mathbf{P}(R)\right)^2 + \mathbf{V}(R) + \frac{\bar{l}(\bar{l}+1)}{2\mu R^2}\mathbf{I}\right]\vec{\psi} = E\vec{\psi} \quad (1)$$

where μ is the reduced mass of the system, the centrifugal term is approximated by an effective diagonal centrifugal barrier, corresponding to an effective orbital angular momentum $\bar{l}$, and the $\mathbf{P}$ matrix accounts for nonadiabatic effects. The orbital angular momentum $\bar{l}$ plays here the role of a parameter, over which, for obtaining integral cross sections, we will eventually sum until convergence.

The diagonal matrix $\mathbf{V}(R)$ contains the eigenvalues of $\mathbf{V}_{el}$ and $\mathbf{V}_{so}$ (of course independent of the diabatic representation chosen):

$$\mathbf{T}(R)[\mathbf{V}_{el}(R) + \mathbf{V}_{so}(R)]\tilde{\mathbf{T}}(R) = \mathbf{V}(R) \quad (2)$$

The elements of diagonal matrix $\mathbf{V}(R)$ are the effective adiabatic potential $V_{|j\ \Omega\rangle}$. As previously suggested,[6,7,23] it is convenient to define a spherical interaction $V_0(R)$ and an anisotropy $V_2(R)$ as

$$V_0 = (2V_\Pi + V_\Sigma)/3 \quad V_2 = {}^2/_3(V_\Sigma - V_\Pi) \quad (3)$$

where the quantities $V_\Sigma(R)$ and $V_\Pi(R)$ are the eigenvalues of the electrostatic Hamiltonian $\mathbf{V}_{el}$; they are labeled by the quantum number Λ, the projection of the electronic angular momentum L on the intermolecular axis, and, as usual, Σ and Π stand for $\Lambda = 0$ and $\Lambda = 1$, respectively.

For a ^{3}P atom collision with a spherical target, the $V_{|j\ \Omega\rangle}$ potentials, obtained by eq 2, are explicitly[9,17b]

$$V_{|2\ 2\rangle} = V_0 - {}^1/_5V_2 \quad (4)$$

$$V_{|2\ 1\rangle} = V_0 + {}^1/_{10}V_2 + {}^1/_2\Delta_1 - {}^1/_2({}^9/_{25}V_2^2 + \Delta_1^2)^{1/2}$$

$$V_{|2\ 0\rangle} = V_0 + {}^1/_{10}V_2 + {}^1/_2\Delta_0 - {}^1/_2({}^9/_{25}V_2^2 + \Delta_0^2 - {}^2/_5\Delta_0V_2)^{1/2}$$

$$V_{|1\ 1\rangle} = V_0 + {}^1/_{10}V_2 + {}^1/_2\Delta_1 + {}^1/_2({}^9/_{25}V_2^2 + \Delta_1^2)^{1/2}$$

$$V_{|1\ 0\rangle} = V_0 - {}^1/_5V_2 + \Delta_1$$

$$V_{|0\ 0\rangle} = V_0 + {}^1/_{10}V_2 + {}^1/_2\Delta_0 + {}^1/_2({}^9/_{25}V_2^2 + \Delta_0^2 - {}^2/_5\Delta_0V_2)^{1/2}$$

where Δ_1 and Δ_0 are the levels of the fine structure multiplet of the ^{3}P atom. In the case of oxygen, $\Delta_1 = 19.6$ meV; $\Delta_0 = 28.1$ meV.

(22) Since at large R values Ω tends to the atomic sublevel projection m_j, the beam direction is the appropriate quantization axis for these experiments (see also note 20).

(23) Reid, R. H. G.; Dalgarno, A. *Phys. Rev. Lett.* **1969**, *22*, 1029. Reid, R. H. G. *J. Phys.* **1973**, *B6*, 2018.

TABLE I: Relative Weights W_{jm_j} of the $|j\ m_j\rangle$ States of O(^{3}P$_j$) at Zero and at High Magnetic Field[a]

$\|j\ m_j\rangle$	zero field	high field	$\|j\ m_j\rangle$	zero field	high field
$\|2\ 2\rangle$	0.251	0.306	$\|1\ 1\rangle$	0.192	0.312
$\|2\ 1\rangle$	0.251	0.000	$\|1\ 0\rangle$	0.096	0.000
$\|2\ 0\rangle$	0.125	0.102	$\|0\ 0\rangle$	0.086	0.280

[a] Atomic projections m_j refer to the beam direction. Under present experimental conditions, they correlate adiabatically with the projections Ω on the intermolecular axis.

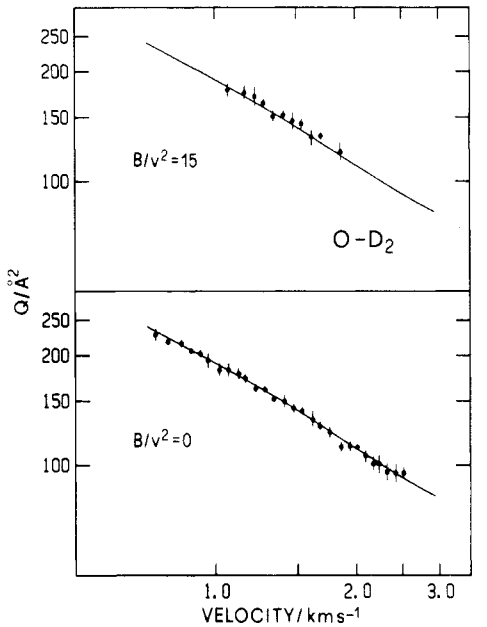

Figure 2. Absolute integral cross sections for the O–D_2 system as a function of the velocity v measured at zero (bottom) and at relatively high (top) magnetic field ($B/v^2 = 15$ in units given in Figure 1). The curves represent the cross sections calculated according to the procedure described in the text.

These eigenvalues $V_{|j\ \Omega\rangle}$ are the effective potential energy curves in the adiabatic representation, eq 1. The coupling between them is represented by the matrix $\mathbf{P}$ whose elements couple states with different j values (but not Ω, which is conserved in this approximation). Accordingly, they will be indicated as $\langle j\ \Omega|\mathrm{d}/\mathrm{d}R|j'\ \Omega\rangle$ and in the case of ^{3}P collision are explicitly given by

$$\langle 2\ 0|\mathrm{d}/\mathrm{d}R|0\ 0\rangle = P_{20,00} = \frac{-10/\sqrt{2}}{9\beta_0^2 - 10\beta_0 + 25}\frac{\mathrm{d}\beta_0}{\mathrm{d}R} \quad (5)$$

$$\langle 2\ 1|\mathrm{d}/\mathrm{d}R|1\ 1\rangle = P_{21,11} = \frac{-15/2}{9\beta_1^2 + 25}\frac{\mathrm{d}\beta_1}{\mathrm{d}R}$$

where $\beta_0 \equiv V_2/\Delta_0$ and $\beta_1 \equiv V_2/\Delta_1$.

In this approach, which is similar to the one used also for studying the interaction of fluorine atoms with rare gases,[10] scattering of oxygen atoms is described by the effective adiabatic curves (4), provided that the nonadiabatic coupling between them is negligible. This will be shown below to be the case by explicit computation of the matrix elements of the $\mathbf{P}$ matrix.

This analysis shows that the measured integral cross section can be given by a weighted sum of cross sections $Q_{j\Omega}(v)$ for scattering by the potentials $V_{|j\ \Omega\rangle}$

$$Q(v) = \sum_{j\Omega} W_{j\Omega}Q_{j\Omega}(v) \quad (6)$$

where the weights $W_{j\Omega}$, which depend on the magnetic field strength, are known (Figure 1 and Table I).

IV. Results and Data Analysis

The absolute integral cross sections $Q(v)$ for O–D_2 and O–CH_4 measured as a function of the beam velocity v are reported in Figures 2 and 3. In the case of the O–CH_4 system the cross

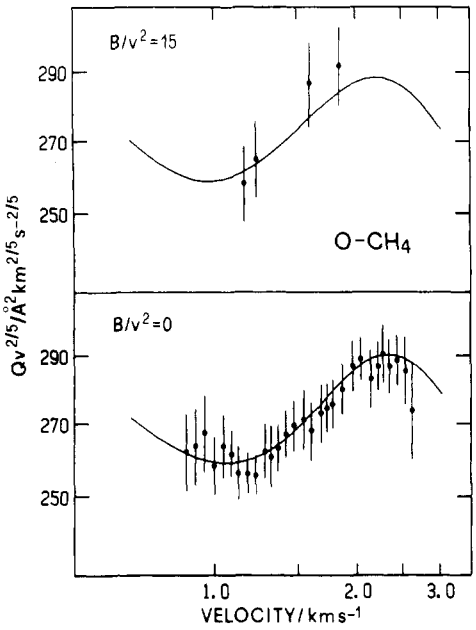

Figure 3. Absolute integral cross sections for the O–CH_4 system as a function of the velocity v measured at zero (bottom) and at relatively high (top) magnetic field ($B/v^2 = 15$ in units given in Figure 1). The curves represent the cross sections calculated according to the procedure described in the text.

sections have been plotted as $Qv^{2/5}$ to emphasize the glory structure. The measurements have been performed at zero and at high magnetic field.

In the case of O–CH_4, because of low signal to background ratios when the magnet was used, only a few measurements could be taken in the region of highest m/e 16 signal. In Table I the relative population W_{jm_j} of the various $|j\ m_j\rangle$ states present in the beam at zero and at a relatively high magnetic field are reported. In the analysis the cross sections have been calculated with eq 6 where the weights $W_{j\Omega}$ are experimentally determined (see Figure 1 and Table I). The total cross sections $Q_{j\Omega}(v)$ have been obtained for the $V_{|j\ \Omega\rangle}$ potentials by using an accurate semiclassical procedure for O–CH_4[24] and the direct summation of JWKB phases for O–D_2. These potentials are produced from eq 4 once V_0 and V_2 are specified.

In the present cases the experimental results are sufficiently accurate to require the use of a flexible potential model for $V_0(R)$. The following Morse–Spline–van der Waals (MSV) parametrization is used, as for O–rare gases,[9] with the consideration that the same model describes satisfactorily the spherical part of the interactions involving methane with other partners:[12,25]

$$x = R/R_m \quad f(x) = V_0(R)/\epsilon \tag{7}$$

Morse:

$$f(x) = e^{-2\beta(x-1)} - 2e^{-\beta(x-1)} \quad \text{for } x \le x_1$$

Spline:

$$f(x) = b_1 + (x - x_1)\{b_2 + (x - x_2)[b_3 + (x - x_1)b_4]\} \quad \text{for } x_1 < x < x_2$$

van der Waals:

$$f(x) = -\left(\frac{C_0}{\epsilon R_m^6}\right)x^{-6} \quad \text{for } x \ge x_2$$

where C_0 is the long-range R^{-6} constant and ϵ and R_m are the well depth and its location. The C_0 coefficient is obtained from the absolute value of the cross section,[24] and the b_1, b_2, b_3, and b_4 parameters of the Spline function are automatically fixed by imposing that the functions have the same value and the same derivative both at x_1 and x_2.

For the term $V_2(R) = {}^5/_3(V_\Sigma - V_\Pi)$ the experiments are mainly sensitive to the short-range repulsive interactions, which decay exponentially. Simple quantum chemical arguments suggest that in this range $V_\Sigma > V_\Pi$. On the other hand, at long range, $V_\Sigma < V_\Pi$ and $V_2(R)$ is mainly due to the polarizability of the oxygen atom.[26] Therefore the following Buckingham-type model has been used in the form

$$V_2 = A_2e^{-\alpha_2 R} - C_2/R^6 \tag{8}$$

The C_2 term is estimated to agree with the anisotropy polarizability of the oxygen atom.[26]

Information on the parameters R_m, ϵ, and β, which characterize the range, strength, and shape of $V_0(R)$ in eq 7, comes mainly from the slope of the cross sections for D_2 and from the glory pattern for methane. The anisotropy parameters A_2 and α_2 in eq 8 are related to the overall behavior of cross sections, including the quenching of the glory amplitude. All these parameters have been varied to obtain the best agreement with the experimental data. In the analysis of the O–CH_4 data the starting potential parameters for the V_0 term are those reported in ref 12. The cross sections calculated in the center-of-mass system have been convoluted in the laboratory system with the procedure described in ref 15. The potential parameters so obtained are reported in Table II, while the calculated cross sections are compared with those measured in Figures 2 and 3.

TABLE II: Potential Parameters for the O(^{3}P)–H_2, CH_4 Systems

	O–H_2	O–CH_4
Spherical Interactions, $V_0(R)$ (Eq 7)		
ϵ/meV	4.7	9.3
R_m/Å	3.49	3.75
β	6.45	6.20
C_0/(meV Å^6)	1.061×10^4	3.844×10^4
x_1	1.12	1.12
x_2	1.55	1.47
b_1	−0.7097	−0.7246
b_2	1.4428	1.6497
b_3	−4.0995	−4.1218
b_4	3.5996	3.1233
Anisotropic Term $V_2(R)$ (Eq 8)		
A_2/meV	2.3225×10^5	6.0842×10^5
α_2/Å^{-1}	2.9298	2.7751
C_2/(meV Å^6)	2.366×10^3	8.546×10^3

V. Discussion

In the analysis of experimental integral cross sections (section IV) the interaction of oxygen atoms with hydrogen and methane molecules has been represented by an effective two-body anisotropic interaction, and the anisotropy, at the distances sampled by these experiments, has been mainly attributed to the atomic open shell structure. For D_2 and CH_4 this amounts to assuming, as is reasonable at the low energies of these experiments, that the system behaves adiabatically with respect to molecular vibration. As far as rotations are concerned, we note that the contribution to the observed anisotropy effects from different orientations of the methane and deuterium molecules plays only a minor role under the experimental conditions of this work. The substantially isotropic behavior of CH_4 has been shown and discussed in ref 12, 15, and 25, whereas for D_2 empirical evidence will be presented in the Appendix of this work. Accordingly, the anisotropy effects observed have been attributed to the intrinsic anisotropy of the open shell structure of oxygen atoms.

Both for the O–H_2 and O–CH_4 systems, the weak long-range interactions obtained by the present technique are much smaller than thresholds for reactive chemical processes, which are of the order of 10 kcal/mol.[11,13,14] These barriers are much higher than

(24) Pirani, F.; Vecchiocattivi, F. *Mol. Phys.* **1982**, *45*, 1003.
(25) Buck, U.; Schleusener, J.; Malik, D. J.; Secrest, D. *J. Chem. Phys.* **1981**, *74*, 1707. Liuti, G.; Pirani, F.; Buck, U.; Schmidt, B. *Chem. Phys.*, in press.
(26) From Werner and Meyer (Werner, H. J.; Meyer, W. *Phys. Rev. A* **1976**, *13*, 13) one has for the relative polarizability anisotropy of the ground-state oxygen atom, $(\alpha_\Sigma - \alpha_\Pi)/\alpha_\Sigma + 2\alpha_\Pi \simeq 0.18$. From the Slater–Kirkwood approximation (Slater, J. C.; Kirkwood, J. G. *Phys. Rev.* **1931**, *37*, 682) this leads to $C_2/C_0 \simeq 0.22$. This value has been used for the two systems.

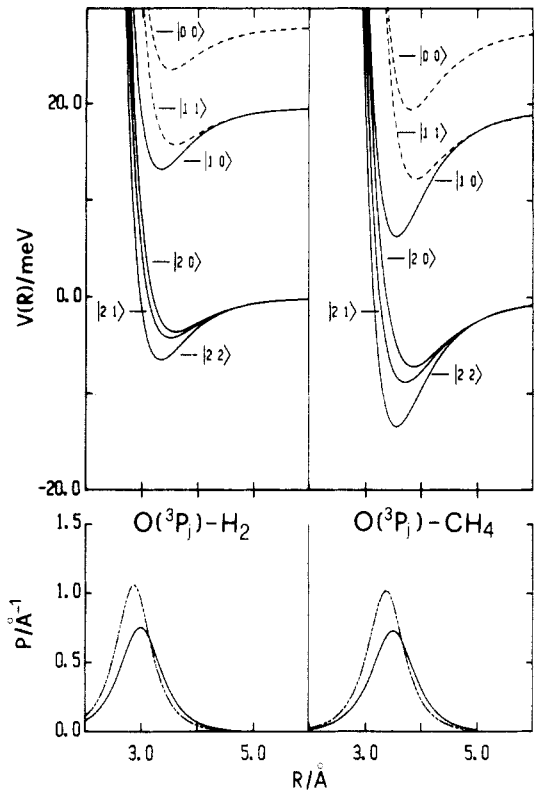

Figure 4. (Upper panels) Adiabatic potential energy curves for the $O(^3P_j)$–H_2 and $O(^3P_j)$–CH_4 interactions as obtained from the analysis reported in this work. The curves are labeled according to the formalism described in the text by using the $|j\ \Omega\rangle$ basis: at long range they tend to the corresponding $|j\ m_j\rangle$ states of $O(^3P_j)$; at short range dashed curves are of Σ symmetry and full curves are of Π symmetry. (Lower panels) Nonadiabatic terms P that couple the $|2\ 0\rangle$ and the $|0\ 0\rangle$ states (dashed curves) and the $|2\ 1\rangle$ and $|1\ 1\rangle$ states (full curves). Maxima of the P functions mark the separation between coupling schemes, the molecular case (a) at short distances and the diatomic case (c) at long range (see text).

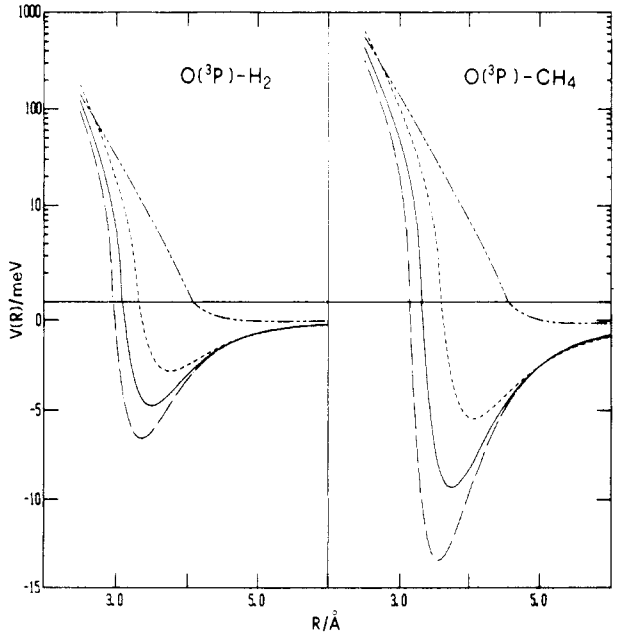

Figure 5. The spherical component V_0 (—), the anisotropic component V_2 (– – –), and the related V_Σ (– · –) and V_Π (– · · –) electrostatic interactions for O–H_2 and O–CH_4 systems.

ranges of potential energy surfaces sampled in this work: the present cross sections are most sensitive to the van der Waals well region determined by a balance between the tail of the repulsion and the long-range attraction.

TABLE III: Some Derived Potential Parameters[a]

		O–H_2	O–CH_4
V_0	ϵ	4.7	9.3
	R_m	3.49	3.75
	σ	3.11	3.33
V_2	ϵ	0.06	0.17
	R_m	5.31	5.61
	σ	4.76	5.03
V_Σ	ϵ	2.8	5.5
	R_m	3.75	4.06
	σ	3.35	3.63
V_Π	ϵ	6.5	13.4
	R_m	3.35	3.56
	σ	2.98	3.15
$V_{\|2\ 1\rangle}$	ϵ	4.3	8.8
	R_m	3.52	3.72
	σ	3.12	3.26
$V_{\|2\ 0\rangle}$	ϵ	3.7	7.2
	R_m	3.60	3.86
	σ	3.21	3.38
$V_{\|1\ 1\rangle}$	ϵ	4.0	7.5
	R_m	3.59	3.91
	σ	3.22	3.51
$V_{\|0\ 0\rangle}$	ϵ	4.6	8.7
	R_m	3.52	3.82
	σ	3.16	3.43

[a] The parameters for $V_{|2\ 2\rangle}$ and for $V_{|1\ 0\rangle}$ are the same as for V_Π; see eq 4. Well depths ϵ, their positions R_m, and zeros of the potentials σ are in meV and Å, respectively. Estimated uncertainties are about 10% for ϵ and 2% for R_m and σ.

TABLE IV: Location and Values of the $P(R)$ Function Maxima

		O–H_2	O–CH_4
$P_{20,00}$	P_{max}/Å^{-1}	1.06	1.02
	R_{max}/Å	2.90	3.40
$P_{21,11}$	P_{max}/Å^{-1}	0.76	0.73
	R_{max}/Å	3.00	3.50

The analysis reported in section IV gives, for the two systems, the six adiabatic effective potential energy curves correlating with the different atomic sublevels of $O(^3P_j)$, which are reported in Figure 4. They are generated by using eq 4 with the V_0 and V_2 potential parameters reported in Table II. In Figure 5 a direct comparison between V_0, V_2, and the related interactions V_Σ and V_Π for each system is reported, while some relevant parameters for all curves are presented in Table III.

In another paper we have characterized the interactions of O–rare gas systems[9] by similar measurements and analysis; interestingly, the potential curves obtained for O–Kr in ref 9 and O–CH_4 in this work are very similar. This is not surprising, since the basic physical properties affecting the interaction are essentially polarizabilities and ionization potentials for the spherical part V_0 and for the anisotropic part V_2, respectively: for CH_4 and Kr both these properties have very similar values.[12] Accordingly, the O–H_2 system presents a behavior intermediate between the systems O–Ne and O–Ar.

An interesting feature obtained by this analysis is given by the nonadiabatic coupling elements $P(R)$ obtained from eq 5 and reported in the lower panels of Figure 4. The maxima of the $P(R)$ functions mark the transition between the diatomic coupling scheme (Hund's case (c)) at long range and a molecular coupling scheme (Hund's case (a)) at short range: they occur when the V_2 term is of order of the fine structure splitting Δ_1 and Δ_0. As shown in Figure 4, the two $P(R)$ functions for each system present different maxima because the $\Omega = 0$ and $\Omega = 1$ coupling terms correspond to different splitting. On the other hand, the maxima for $\Omega = 0$ matrix elements are higher than the ones for $\Omega = 1$ because they describe the coupling between curves that have a less prominent molecular (i.e. either Σ or Π) character. Table IV reports values and positions of the maxima of the $P(R)$ functions, and in the case of O–CH_4, they are shifted at larger distances than for O–H_2; this is due to a higher contribution of the anisotropy to the interaction. For O–H_2 the well depths obtained from the present analysis are described in the Hund's

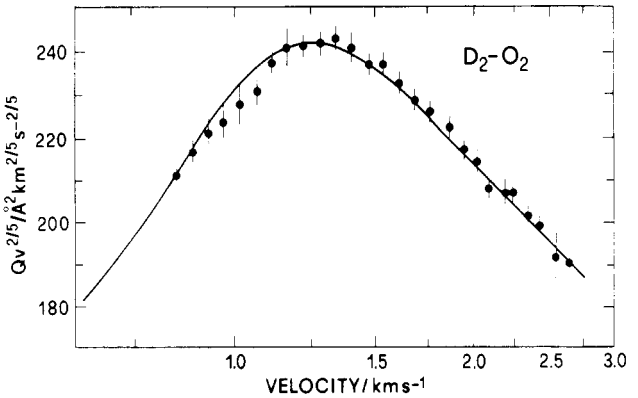

Figure 6. Absolute integral cross sections Q for the D_2–O_2 system as a function of beam velocity. The full curve is the cross section calculated by using a MSV potential model (see Appendix).

TABLE V: MSV Potential Parameters for the O_2–H_2 System

ϵ/meV	5.9	x_2	1.42
R_m/Å	3.60	b_1	−0.7815
β	6.3	b_2	1.7903
C_6/(meV Å^6)	1.853×10^4	b_3	−4.2073
C_8/(meV Å^8)	9.267×10^4	b_4	4.7350
x_1	1.10		

case (c), while for O–CH_4 the maxima of $P(R)$ occur at distances nearer to the minima locations. Therefore the O–CH_4 system presents a more prominent molecular character at the distance around the minima of the potentials.

The $P(R)$ terms are also useful in estimating nonadiabatic effects and in obtaining the first-order nonadiabatic corrections to the adiabatic curves derived in section IV from eq 4. From the values in Table IV it can be seen that these corrections, which are $(\hbar^2/2\mu)P^2$, are well within the uncertainties stated for the present analysis and confirm the adequacy of the adiabatic decoupling scheme used in the analysis of this experimental data. Finally, the dependence on the inverse of reduced mass of the nonadiabatic correction points at a further advantage of using D_2 rather than H_2 in investigating molecular hydrogen interactions.

Acknowledgment. This work has been supported by grants from the Italian Ministero della Pubblica Istruzione and from the Italian Consiglio Nazionale delle Ricerche.

Appendix

Integral Cross Sections for D_2–O_2 Collisions and the Spherical Interaction between Hydrogen and Oxygen Molecules. In Figure 6 the absolute integral cross sections Q of the D_2–O_2 system (plotted, as usual when in the glory region, as $Qv^{2/5}$) are reported as a function of the beam velocity v. These measurements have been performed mostly to obtain a calibration for the absolute scale of the cross sections of this work (see section II and also ref 12).

For the analysis a MSV potential model is used (see eq 7 in section IV). The quality of the data allows one to take into account also the long-range dipole–quadrupole interaction described by C_8/R^8 in addition to the dipole–dipole interaction described by a C_6/R^6 term. The potential parameters are reported in Table V and can be shown to fit into the picture of the weak intermolecular forces that is known at present. The capability of a spherical potential model to reproduce the large and well developed glory structure observed for this system (Figure 6) indicates that, under the present experimental conditions, namely at a relatively high rotational temperature of the particles involved, a substantially isotropic interaction drives the collision between these molecules. This can be taken as empirical evidence for excluding contributions from molecular rotations to the anisotropy effects discussed in the paper and attributed to the open shell structure of the oxygen atom.

Registry No. O, 17778-80-2; H_2, 1333-74-0; CH_4, 74-82-8; O_2, 7782-44-7.

Deuterium Isotope Effects on S_1 Radiationless Decay in Phenol and on Intermolecular Vibrations in the Phenol–Water Complex

Robert J. Lipert and Steven D. Colson*

Sterling Chemistry Laboratory, Yale University, New Haven, Connecticut 06511 *(Received: April 11, 1988)*

Replacement of the phenol OH hydrogen with deuterium has been found to reduce the rate of internal conversion in the supersonic jet cooled molecule by over 2 orders of magnitude. A similar but less pronounced effect was previously observed when water is hydrogen-bonded to the same hydrogen. It is likely that both effects are caused by a reduction in the effectiveness of the OH vibration in acting as an accepting mode in radiationless transitions due to a lowering of its vibrational frequency. The multiphoton ionization (MPI) spectra of phenol–water complexes containing one, two, or three deuteriums confirm the assignments of two low-frequency intermolecular vibrations. Successive shifts of the hydrogen bond stretching vibration as deuteriums are substituted into the complex have been used to determine the sites at which the substitution is occurring. Fermi resonances involving the hydrogen bond stretching vibration were also found in some isotopic species.

Introduction

Through the study of radiationless transitions in supersonic jets, it has recently been established that the rate of internal conversion from the S_1 to the ground state of the phenol–H_2O complex is much lower than in free phenol.[1,2] It has been suggested[1] that this is because a phenol OH vibration or vibrations are less effective accepting modes due to the hydrogen bonding of water to the hydrogen of the phenol OH. These vibrations are attractive candidates for accepting modes since they are either of high frequency or undergo large frequency shifts between the ground and S_1 states. For example, the 3656-cm^{-1} ground-state OH stretching frequency is the highest frequency vibration in phenol[3,4] and may therefore be the most important accepting mode. It is well established that the OH stretching frequency is lowered by hydrogen bonding in which phenol acts as the proton donor,[5] as

(1) Sur, A.; Johnson, P. M. *J. Chem. Phys.* **1986**, *84*, 1206.
(2) Lipert, R. J.; Bermudez, G.; Colson, S. D. *J. Phys. Chem.* **1988**, *92*, 3801.
(3) Bist, H. D.; Brand, J. C. D.; Williams, D. R. *J. Mol. Spectrosc.* **1967**, *24*, 402.
(4) Bist, H. D.; Brand, J. C. D.; Williams, D. R. *J. Mol. Spectrosc.* **1967**, *24*, 413.

0022-3654/89/2093-0135$01.50/0